Available online at www.sciencedirect.com
ScienceDirect
Journal of Sound and Vibration 307 (2007) 698–719
JOURNAL OF SOUND AND VIBRATION
www.elsevier.com/locate/jsvi

Vortex-induced vibration effect on fatigue life estimate of turbine blades

Y.L. Lau, R.C.K. Leung*, R.M.C. So

Department of Mechanical Engineering, The Hong Kong Polytechnic University, Hung Hom, Kowloon, Hong Kong

Received 12 October 2006; received in revised form 21 June 2007; accepted 30 June 2007
Available online 11 September 2007

Abstract

An analysis of a turbine blade fatigue life that includes the physics of fluid–structure interaction on the high cycle fatigue (HCF) life estimate of turbine blades is carried out. The rotor wake excitation is modeled by rows of Karman vortices superimposed on an inviscid uniform flow. The vortex-induced vibration problem is modeled by a linear cascade composed of five turbine blades and the coupled Euler and structural dynamics equations are numerically solved using a time-marching boundary element technique. The analysis can be applied to any blade geometries; it is not limited to the blade geometry considered here. Two major design parameters have been identified; the ratio of blade spacing to blade chord length s/c of the stator, and the normalized frequency parameter c/d which is related to the wake passing frequency of the rotor. For a rigid cascade, it is found that aerodynamic resonance prevails at the resonant c/d values corresponding to an isolated blade while s/c is responsible for the level of the aerodynamic response. If the central blades were elastic, the parameter s/c plays a different role in the fluid–structure interaction problem. With a c/d that could lead to structural resonance for an isolated blade, changing s/c would stabilize the aerodynamic and structural response of the elastic blade in a cascade. On the contrary, an improper choice of s/c might turn the elastic blade response into structural resonance even though the oncoming c/d is non-resonant. The results of the nonlinear effects of c/d and s/c could be used together with the Campbell diagram to obtain an improved HCF design of rotor–stator pair.

1. Introduction

The design of rotor–stator pairs in axial-flow turbomachine has advanced to the stage where further improvements have to derive from a better understanding of the occurrence of fluid–structure interaction and the eventual control of blade unsteady aerodynamics. Unsteady aerodynamics is the main source that drives the rotor and stator blades into destructive vibration modes, which could lead to high cycle fatigue (HCF) structural failure of the blades after long exposure to unsteady loading. A major concern of axial-flow turbomachine design is the minimization of the structural vibration of rotor/stator blades induced by unsteady wake flow when the turbomachine is in operation. The common design approach against blade vibration is to

*Corresponding author. Tel.: +852 2766 6645; fax: +852 2365 4703.
E-mail addresses: yllau@spinmaster.com.hk (Y.L. Lau), mmrleung@inet.polyu.edu.hk (R.C.K. Leung), mmmcso@polyu.edu.hk (R.M.C. So).

0022-460X/$ - see front matter © 2007 Elsevier Ltd. All rights reserved.
doi:10.1016/j.jsv.2007.06.029

Nomenclature

a	distance between the elastic axis and the center of mass of the blade
BEM	boundary element method
c	blade chord length
d	spacing of oncoming vortices
C_L, C_D, C_M	lift, drag and moment coefficients
C_P	pressure coefficient
$\hat{e}_{y1}$	unit vector in streamwise y_1 direction
FFT	fast Fourier transform
f_r	rotational frequency of the rotor, Hz
h	plunging displacement
HCF	high cycle fatigue
i	index
IGV	inlet guide vane
k_h	bending stiffness
k_θ	torsional stiffness
K	material constant
KVS	Karman vortex street
L	unsteady aerodynamic lift$=(1/2)C_L\rho U_\infty^2 c$
m	mass of blade section per unit span
M	unsteady aerodynamic moment$=(1/2)C_M\rho U_\infty^2 c$
N	number of cycles to fatigue failure
N_r	number of rotor blades
$\hat{n}$	normal vector
(n_{y1}, n_{y2})	components of outward normal in y_1 and y_2 directions
P	power spectral density
$\Re$	design rotor speed, rev/min
Re	Reynolds number $= U_\infty c/\nu$
s	blade spacing of stator disk
s_{ax}	axial spacing between rotor and stator disks
t	dimensional time
U_∞	free-stream velocity
U_{conv}	convection velocity of rotor wake disturbance
V	velocity vector
V_0	convective velocity generated by the inviscid flow
V_S	velocity of blade surface
V_ω	rotational part of V_0
x	position vector
WPF	wake passing frequency
(y_{1p}, y_{2p})	position of blade center of mass

Greek symbols

α_i, α_o	inlet and outlet flow angle
Γ	circulation of vortex
γ	arc length of blade surface profile
δt	dimensionless time step
Θ	lift ratio
θ	torsional deformation, positive nose up
λ	stagger angle of the rotor or stator blade
ν	kinematic viscosity
ρ	fluid density
σ	stress amplitude
τ	dimensionless time $= U_\infty t/c$
ω	vorticity $= \nabla \times V$
ω_i	ith structural natural frequency

Superscripts and subscripts

$\dot{}$	first time derivative
$\ddot{}$	second time derivative
$(\,)_{rms}$	root mean square value

choose the optimal combination of operational and geometric parameters of the rotor–stator pair so that blade vibration is reduced to a minimum. Operational parameters are those design attributes that change with the time-varying load requirements under various working conditions. This is commonly achieved by adjusting the rotational frequency f_r of the rotor. Geometric parameters are those design values that, once designed, will not change regardless of the turbomachine operating conditions and they are usually linked to geometric definitions of the turbomachine components such as: (i) chord length c of the rotor or stator blade; (ii) number N_r of blades in the rotor or stator disk; (iii) axial spacing s_{ax} between the rotor and stator disk; (iv) stagger angle λ of the rotor or stator blade; (v) profile of the blade section; and (vi) blade spacing s of the rotor or stator disk.

The configuration of a rotor–stator pair involves numerous operational and geometric parameters such as λ s_{ax}/c, s/c, $U_\infty/N_r f_r$ and other parameters of lesser importance; therefore, it is common practice to reduce the number of relevant parameters by forming dimensionless groupings and study their mutual relationships. In their cascade aerodynamic analysis, Hill and Peterson [1] found that α_o is a function of α_i, s/c, and λ. Rao [2]

found that the perturbations encountered by the stator blades are pulsating at a frequency, WPF $= N_r f_r$, dictated by the passage of upstream rotor blades cutting across the stator blades. The WPF also determines the structural vibration, the unsteady aerodynamics and the aeroacoustic behavior of the downstream stator blades [3,4]. So et al. [5] modeled the wake disturbance as rows of alternating Karman vortices (KVS) convected by U_∞ and found that a key parameter is c/d. This parameter, also known as the normalized wake passing frequency, follows naturally from a dimensional analysis of the governing equations using U_∞ and c as the characteristic velocity and length scale and choosing the characteristic frequency as U_∞/d.

In a theoretical study, Sanders and Fleeter [6] changed the s_{ax}/c of a stator–rotor–stator configuration and examined the resultant unsteady lift and moment of the rotor disk blades. They found that the levels of the unsteady lift and moment of the rotor blades could be significantly reduced by indexing the stator vanes at close axial spacing; the reduction is particularly prominent at high Mach numbers. This concept was then extended to inlet guide vane (IGV)–rotor pair in transonic axial-flow compressor [7–9]. These experiments showed that the unsteady aerodynamic loading acting on the IGV blades resulting from IGV–rotor interactions could be affected by changing the s_{ax}/c of the IGV–rotor; the larger the s_{ax}/c, the steadier the aerodynamic load acting on the IGV blades. In addition, the phase of the upstream pressure fluctuations is remarkably affected by the IGV–rotor axial spacing [8]. The results support the numerical prediction that the aerodynamic unsteadiness of the stator blade passage increases with a smaller spacing between the rotor–stator pair and a smaller wake/blade count ratio, and consequently an increase in time-averaged loss coefficient [10]. Furthermore, Fleeter et al. [11] found that decreasing s_{ax}/c could reduce the level of the unsteady pressure fluctuation on the stator blades.

Another important geometric parameter in rotor–stator design is s/c. Mellor [12,13] studied the effect of s/c in axial flow compressors and found that α_o was affected by s/c. Emery et al. [14] examined the performance of a NACA 65-series compressor blade section in a cascade with subsonic uniform inflow; their results showed that the lift coefficient of the cascade blades is a function of s/c, blade camber, α_i and the flow turning angle. Yilbas et al. [15] used the control volume method and a k–ε turbulence model to simulate the development of flow passing through a cascade of NACA 0012 airfoils with special attention on solidity effects, i.e. c/s and λ. Their results revealed that an increase in cascade solidity results in an increase in the angle of incidence at which maximum lift occurs, accompanied by a mild increase in drag. Dobrzynski [16] experimentally studied the effect of s/c between propeller blades and its noise generation. His experiments clearly showed that the use of asymmetrical blade arrangement for propeller was able to achieve a noise reduction up to 4 dB as compared with the same propeller with uniform blades.

Since c/d is closely tied to the external forcing function in flow-induced vibration of stator blades, it is an important operational parameter in rotor–stator design. For an isolated blade, or airfoil, subject to oncoming parallel rows of alternating vortices arranged in a KVS pattern, it was found that the flow-induced vibration and aeroacoustic behavior of the vibrating structure could be characterized by c/d of the KVS, regardless of the geometry of the structural section profile [5,17]. Furthermore, their studies showed that the fluctuations of the aerodynamic loading on a rigid blade follow the oncoming vortical excitation and attain peak values at discrete values of c/d such as 0.5, 1.5 and 2.5. This phenomenon was termed aerodynamic resonance. If the blade is elastic, the structural response will resonate at another set of discrete frequencies, leading to the occurrence of structural resonance. The structural resonant frequencies generally show a shift from the natural frequencies of the structure *in vacuo* and critically depend on the interactions of the entire fluid–blade system. The aeroacoustic responses of an elastic blade undergoing aerodynamic or structural resonance are the highest due to the strongest aerodynamic fluctuating loads acting on the blade under these conditions [17].

Once the relationship between the aerodynamic and aeroacoustic performance and the geometric and operational parameters of a rotor–stator pair is known, it is a natural step to construct design criteria which consisted of sets of curves that facilitate design parameter selection of axial-flow turbomachines to deliver the desired efficiency and performance. The Mellor-NACA charts [12,13] are among the earliest design curves for steady cascade aerodynamics that relate α_o, α_i, λ and solidity of a series of cascade composed of NACA 65 series airfoils. For single-stage compressors and fans with NACA 65 series blade sections and settings, Mellor-NACA charts enable turbomachinery designer to select the desired α_o and α_i that allow the cascade to operate between positive and negative stall limits. Similarly, with NACA 65 series airfoils, Emery et al. [14] provided continuous variations of blade section performance with respect to such cascade parameters as the blade

camber, α_i, and solidity. Their summary charts enable compressor designers to select the proper blade camber and α_i based on the velocity diagram of a single-stage compressor and predetermined solidity. In addition, having determined the useful section operating range in terms of camber and α_i, the charts provide a simple method to obtain the off-design variation in turning angle. Johnsen and Bullock [18] presented design curves that defined the relationship between the total pressure-loss coefficient of a cascade blade section, the inlet Mach number, incidence angle, solidity and the blade section geometry of a cascade, while Kacker and Okapuu [19] indicated that the total-to-total efficiency, defined as the ratio of the actual to the ideal enthalpy difference between stages, of a turbine is strongly related to the stage work and axial flow velocity.

Other sets of design criteria for axial-flow turbomachines are constructed to assess the dynamic phenomena due to unsteady flow through the blade passage, such as the stability margin for flow-induced vibration. One of the most popular sets is the Campbell diagram which provides guidelines to the selection of the number of blades in a rotor–stator pair so that the resonant operating conditions, created by the coincidence of upstream rotor disk WPFs and the natural frequencies of downstream stator blades, of the pair can be avoided. Alternatively, Fottner [20] has outlined a margin region expressed in terms of a pressure ratio and mass-flow for fans and compressors. As long as the fans/compressors are operating inside the region, many dynamic phenomena, such as several types of blade flutter, subsonic/transonic-stall flutter, choke flutter, low- and high-incidence supersonic flutters, and supersonic-bending stall flutter, can be prevented.

In spite of the importance of the s/c and c/d parameters in the flow around elastic blades, little work has been carried out to incorporate their effects into the design criteria of axial-flow turbomachines. The brief review above shows that the s/c and c/d effects are, to a great extent, the consequence of fluid–structure interaction between the flow and the blade responses. Therefore, if these effects were to be considered, an analysis that takes fluid–structure interaction into account has to be carried out. As a first attempt, an inviscid flow is considered and this means that the fluid–structure interaction is accounted for through the tangency condition, i.e., only the elastic effect of the blade on the flow and hence the shed vortices are considered. The viscous effect is neglected in this initial attempt. Once the s/c and c/d effects are determined, they are used in conjunction with the Campbell diagram so that their effects could also be included in the eventual design of axial-flow turbomachines.

It is now clear that the first objective of the present study is to examine the effect of c/d and s/c of a coupled rotor–stator pair on the unsteady aerodynamic response and the vibration of the blades in the stator. In the present analysis, s_{ax} and U_∞ are fixed for all cases and the normalized blade aerodynamic and structural responses due to the coupled vortex–blade interactions are compared in a relative sense. Based on the results of the first objective, the second objective is to devise practical design curves for the estimate of blade fatigue life that accounts for the interaction of c/d and s/c. It is hoped that the design curves could help turbomachinery designers to more accurately predict the occurrence of aerodynamic and structural resonance with respect to c/d and s/c and assess their effect on the vortex-induced vibration of a stator blade and their combined impact on the blade fatigue life. This approach is rather generic because it is not limited by the geometry of the blades; the analysis can be carried out with any blade geometry.

2. Formulation and fatigue life estimate

Four models are required for the present analysis of vortex-induced vibration and its effect on HCF life estimate of stator blades in a rotor–stator pair. Three of the models focus on the aerodynamics and structural dynamic analysis and the fourth is on fatigue life estimate. These models are: the cascade model to simulate the flow in a rotor–stator pair, the wake excitation model, the fluid–structure interaction model and the HCF life estimate model. Each model is briefly discussed below.

2.1. Cascade model

As a first attempt, the present study assumes a two-dimensional (2-D) cascade model, which is formed by cutting the circumference of the stator blade disk and then stretched it out to form a linear cascade with N_r number of blades. The 2-D analog provides a convenient testing ground for the vortex–blade interaction while retaining the essential physics of the full 3-D interaction.

Theoretically, the linear cascade should comprise an infinite number of blades so as to correctly represent the intrinsic flow periodicity that the blades experience. However, for a blade disk running steadily without stall, all of its blades should essentially experience the same fluctuating aerodynamic loads and give the same structural responses in every disk revolution. Therefore, it is sufficient to focus on only one single blade and its flow-induced vibration. A finite number of neighboring blades are placed around the single blade to replicate the periodic boundary conditions. The selection of the number of neighboring blades of a finite cascade are guided by the deviation of the steady lift ratio Θ from its corresponding infinite counterpart. Lau [21] has computed the steady aerodynamics of a linear cascade with five blades using boundary element method (BEM) and compared the results with the linear theory of Wislicenus [22]. A brief description of the BEM is given in Section 2.2 below. The maximum error in Θ of the central blade is only 1.6% for an s/c range between 0.6 and 2.4. Speziale et al. [23] used five NACA 0012 airfoils, cambered and uncambered, to investigate the propagating stall in a cascade. The cascade model was able to identify the s/c and α_i range for the propagating stall to occur. The finding was in fair agreement with experimental results. Therefore, a five-blade representation is adopted in the present study.

In order to study the effects of fluid–structure interaction in a cascade systematically, three configurations of cascade model are considered. The first configuration, denoted as Cascade 1, comprises of five rigid blades; the response of the central blade is purely aerodynamic and serves as a baseline for the assessment of fluid–structure interaction effect. The central blade is taken to be elastic in Cascade 2. This configuration allows the flow-induced vibration in the presence of rigid neighboring blades to be examined. The third configuration, denoted as Cascade 3, is one with three elastic central blades and two outer rigid blades. This setup allows the effect of vibrating neighboring blades to be considered. The blade geometry adopted in this study is a high loading turbine blade (T1) and the structural properties assumed are typical of turbomachinery applications [5].

2.2. Rotor wake excitation model

In the present analysis, the rotor wake is considered as the major extraneously induced excitation (EIE) on the stator blades [24]. In general, the main features of the rotor wake disturbance may be considered as a series of vortices periodically shed from the trailing edges of moving rotor blades. These vortices then travel through the passage between two adjacent stator blades. The characteristics of the wake disturbance resemble the form of a periodic and discrete vortex street pattern similar to KVS [25,26]. Furthermore, in a series of experiments dedicated to study the time-varying wake flow characteristics behind turbine blades at high Reynolds number in a Mach number range from 0.4 to 0.79, Cicatelli and Sieverding [27] and Sieverding et al. [28] showed that the wake behind the trailing edge of a turbine blade is essentially characterized by large-scale periodic KVS and the vortex patterns persist regardless of the boundary layer state on the blade surfaces [29]. On the other hand, Hodson [30] demonstrated in his numerical study that, for a subsonic inflow, the rotor-wake–stator interactions were dominated by inviscid mechanisms, rather than by viscous effects. Consequently, the present study adopts a KVS vortex pattern superimposed in an inviscid oncoming stream to model the wake disturbance generated from the rotor blade trailing edge.

Six rows of alternating discrete vortices are superposed on the uniform upstream flow in order to expose each blade in the cascade to a KVS (Fig. 1a). Based on the experimental findings on the shape of the wake defect in turbomachinery applications gathered by Korakianitis [31], the distance between the upstream source of perturbation and the downstream blades is approximately equal to one chord length. Therefore, the release points of the discrete vortices are located at one chord length upstream of the leading edge of the blades. Having set the release points together with a normalized circulation strength Γ (corresponding to $0.5C_L$) of the vortices (of a KVS with magnitude $= 0.1$), it follows that the amplitude of the wake defect function is about $0.07U_\infty$. This choice compares favorably with the data of Korakianitis [31]. The spacing s_v between the release points of the vortex rows in the y_2 direction is so chosen that every vortex is able to pass through the middle of the blade passage at the leading edge plane. Scaling arguments show that the upstream KVS excitation is characterized by c/d. This ratio is related to the rotational speed of the preceding rotor [2] by $d = U_\infty/N_r f_r$.

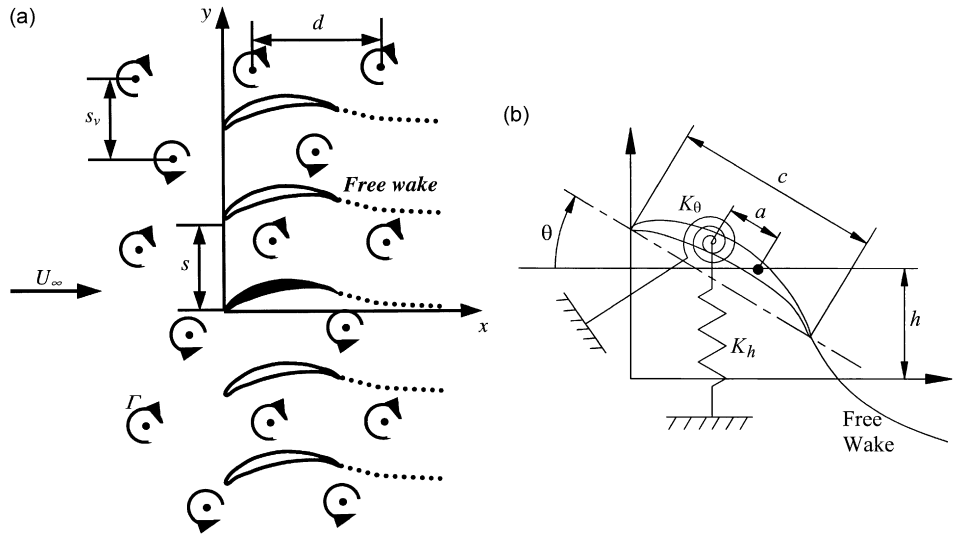

Fig. 1. Schematic of the two-dimensional linear cascade model.

2.3. Modeling fluid–structure interaction

The fully coupled fluid–structure interaction between the blades and the flow non-uniformities are resolved by the time-marching BEM methodology proposed by Jadic et al. [32] and So et al. [5]. The BEM ensures coupling between unsteady aerodynamics obtained by the BEM and structural dynamics integration at every time step so as to correctly resolve the effect of fluid–structure interaction. Complete formulation of the BEM has been given in these papers; therefore, the numerical method is only briefly outlined below.

The unsteady flow field is assumed to be incompressible, inviscid and governed by the 2-D Euler equations. The equations are made dimensionless by U_∞ and c. The transport equation for the vorticity is deduced by taking the curl of the Euler equations. The circulation Γ around a given material curve in the flow field is assumed constant during each time step δt. Consistent with this approach, it is also assumed that, during each time step, the vorticity is essentially frozen and is convected by the inviscid flow. The blades are simulated by a distribution of bounded sources and discrete vortices and the unsteady Kutta condition is imposed at the trailing edges of the blades to accurately determine the vorticity distribution at the trailing edges [32]. Tangency condition $(V_0 - V_S)\hat{n} = 0$ is applied on the surface of all blades. The far-field boundary condition is given by $V_0 = U_\infty \hat{e}_{y_1} + V_\omega$. A free-wake model is used to satisfy the unsteady Kutta condition at all blade trailing edges (Fig. 1b). Once the velocity and pressure fields are known, the unsteady aerodynamic lift (L) and moment (M) on the individual blades can be determined by integrating around the respective blade surface. Their respective coefficients, C_L and C_M, are given by

$$C_L = -\oint [-C_p(\gamma) n_{y1}(\gamma) \sin\alpha + C_p(\gamma) n_{y_2}(\gamma) \cos\alpha]\, \mathrm{d}\gamma, \tag{1}$$

$$C_M = \oint \left\{ [y_1(\gamma) - y_{1p}] C_p(\gamma) n_{y_2}(\gamma) - [y_2(\gamma) - y_{2p}] C_p(\gamma) n_{y_1}(\gamma) \right\} \mathrm{d}\gamma, \tag{2}$$

where $L = (1/2) C_L \rho U_\infty^2 c$ and $M = (1/2) C_M \rho U_\infty^2 c^2$.

It is assumed that the dynamic responses of the blades are governed by a simple two-degree-of-freedom (2-dof) model (Fig. 1b) where the equations of motions are given by

$$m\ddot{h} - ma\cos\theta\ddot{\theta} + k_h h + ma\sin\theta\dot{\theta}^2 = L, \tag{3}$$

$$I\ddot{\theta} - ma\cos\theta\ddot{h} + k_\theta\theta = M. \tag{4}$$

The flow over the blades and their structural responses are coupled to each other through the no-slip or tangency boundary conditions. This nonlinear coupling involves the influence of blade motions on the aerodynamic flow which, in turn, affects the blade structural responses. In order to account for the coupled fluid–structure interaction, at each time step, the flow governing equations and the structural dynamic equations are solved simultaneously in an iterative manner until the relative error of h and θ between successive iterations is less than 10^{-6} [32].

2.4. Fatigue life estimate model

Resonant conditions encountered in turbomachines might give rise to HCF failure of an elastic blade due to cyclic loading accumulated over a period of time. The estimation of blade fatigue life is generally based on the concept of cumulative fatigue damage [33], which states that the total damage incurred by superposing different simultaneous cyclic loadings is identical to the sum of the individual damages produced by the same loadings acting sequentially. The number of cycles that the vibrating structure will last under cyclic loading of constant stress amplitude can be estimated from the S–N curve

$$N = (\bar{\sigma}/\sigma)^{1/K}, \tag{5}$$

where $\bar{\sigma}$ and K are material constants. Assuming that the blade material is "S96" steel, the corresponding corrosion fatigue curve relating fatigue stress strength σ and N leads to a value of $K = 0.2558$ for the stator blades [34]. Since assessing the relative fatigue life of the structure is of primary interest to the present study, it is not necessary to determine the value of $\bar{\sigma}$. In mathematical terms, Miner's rule states that when fatigue failure occurs,

$$\sum_{i=1}^{S} D_i = \sum_{i=1}^{S} \frac{n_i}{N_i} = 1, \quad i = 1, 2, 3, \ldots, S, \tag{6}$$

where the individual damage D_i is given by the ratio of the actual number of cycles performed (corresponding to the ith cyclic stress amplitude and its associated frequency) to the number of cycles that would lead to fatigue failure if that cyclic stress component was acting alone. An estimate of fatigue life can then be determined from the equation

$$T = 2\pi / \sum_{i=1}^{S} \frac{\omega_i}{N_i}, \tag{7}$$

obtained by combining Eqs. (5) and (6). It should be noted that the summation appearing in the denominator of Eq. (7) should be limited to the time-stationary mode of the blade response because, during the service life of a turbomachine, the transient response is comparatively short and will only generate small damages. Therefore, fatigue life estimate is based on the application of Miner's concept to the structural models of the blades. Due to the fact that the detailed geometry of the blade has been lost in this method and the corresponding stress distribution cannot be recovered exactly, the application is not exact. However, it is still possible to compare the fatigue lives of the stator blade obtained under fluid–structure interaction conditions with different combinations of c/d and s/c by substituting the equivalent stress $\sigma_{\mathrm{eq}}(t) = \sqrt{(k_h)h^2(t)/2 + (k_\theta)\theta^2(t)/2}$ for σ. Thus obtained, the actual value of the fatigue life of the stator blade will not be accurate; however, for identical blades, the ratio of two estimated values of fatigue life obtained in connection with two different situations is reliable and credible. In other words, fatigue life estimates are examined in a relative sense rather than in an absolute sense. This analysis is sufficient to highlight the importance of taking fluid–structure interaction into account in HCF estimate.

In assessing fatigue life using Eq. (7), an appropriate cycle identification scheme is needed to extract the frequencies and stress amplitude associated with each cyclic component from the time history of the applied cyclic loadings [35]. If the loading is periodic, these quantities are readily extracted from spectral analysis of the time history using fast Fourier transform (FFT)-based or ARMA-based technique [5]. However, for

irregular loading time history that most engineering structures experience, more sophisticated cycle counting schemes that are able to resolve both large and small stress excursions simultaneously should be used [35]. A list of standard practices for cycle counting in fatigue analysis has been complied in ASTM standard [36]. In the present study, the simplified rainflow counting algorithms proposed by Downing and Socie [37] is adopted.

3. Range of s/c and c/d

One of the objectives of the present study is to establish design curves for axial-flow turbomachines so that s/c and c/d for an operating coupled rotor/stator pair can be selected to minimize the flow-induced vibration effect on blade fatigue life. The design criteria should be formulated to cover practical ranges of s/c and c/d. For this purpose a survey of typical axial-flow turbomachines, mainly aero-engines, has been conducted. Since the technical specifications of the different stages of rotor–stator pairs in aero-engines are strictly confidential, in the present study, all necessary operational and geometric parameters are extracted only from available public information [1,38–41]. The estimate of s/c and c/d of stators/guide vanes are outlined below.

The parameter s/c represents the ratio of the spacing between blades to its chord length. However, in real aero-engines, different flow conditions in turbine and compressor stages require different blade disk sizes and chord length of the blades. Therefore, s/c varies along the axis of disk rotation as well as along the span. In order to simplify the analysis, the mid-radius s/c of a blade disk is taken as the representative value for the input to the cascade analysis. The parameter c/d represents the ratio of chord length to the characteristic wavelength of the vortical disturbances in the rotor wake. Generally, c/d could be estimated from $(c/U_{\mathrm{conv}})(N_r\Re/60)$. Since c varies from stage to stage, engine to engine, and cannot be estimated from the available literature, an approximate value of 0.07 m estimated from the stators of the different stages of the General Electric CF6 turbofan engine is adopted (Kroes and Wild, 1995). In the absence of shock and stall, U_{conv} is more or less constant. The survey results are compiled and summarized in Lau [21]. A realistic range of s/c and c/d for the present study is $0.5<c/d<1.43$ and $1<s/c<5$. Six c/d values (0.5, 0.69, 1, 1.25, 1.4 and 1.43) and nine s/c values at a uniform increment of 0.5 are chosen for the present calculations.

4. Discussion of cascade results

The BEM methodology has been successfully validated by comparing the numerical results with experimental measurements of selected blade–vortex interaction problems. They include the approach of an isolated vortex towards a rigid NACA 0012 airfoil, flow-induced vibration of an elastic NACA 0012 airfoil in a cylinder wake, and the flow-induced vibration of a NACA 0012 airfoil due to double KVS rows generated from two upstream parallel cylinders. Details of these validations are given in Lau et al. [42] and Luk et al. [43]. The BEM was able to replicate the aerodynamics and structural responses of the airfoil and the predictions agree favorably with experimental measurements in all cases investigated. Furthermore, Lau [21] has computed the steady aerodynamics of a linear cascade with five blades using BEM and the results were found to be in good agreement with the linear theory of Wislicenus [22]. This means that the BEM can be used to analyze the present problem with confidence. As before, 5000 time steps with $\delta t = 0.05$ are used for all computations. This time period is long enough for the transients to decay completely and the aerodynamic and structural responses to achieve time-stationary state. The dimensionless strength of the KVS vortices is set equal to ± 0.1 and U_∞ is taken to be 100 m/s. In this section, discussion will focus on the root mean square (rms) aerodynamic and structural response of the central blade, and its stable forced response.

4.1. Aerodynamics of Cascade 1

There is no blade motion in Cascade 1; therefore the response of the central blade is purely aerodynamic. It is clear from Fig. 2 that the aerodynamic response of the blade is a function of c/d and s/c. Peak $(C_L)_{\mathrm{rms}}$ values are found for all c/d. As all blades in Cascade 1 are rigid, the variation in C_L is simply a result of periodic aerodynamic excitation due to the oncoming KVS. The peak $(C_L)_{\mathrm{rms}}$ values manifest aerodynamic resonance as described in So et al. [5]. The s/c value where aerodynamic resonance occurs varies. For example, at $c/d = 0.5$, the value of $(C_L)_{\mathrm{rms}}$ varies slightly in the region where $s/c<1.5$, attains a mild peak at $s/c = 2.5$,

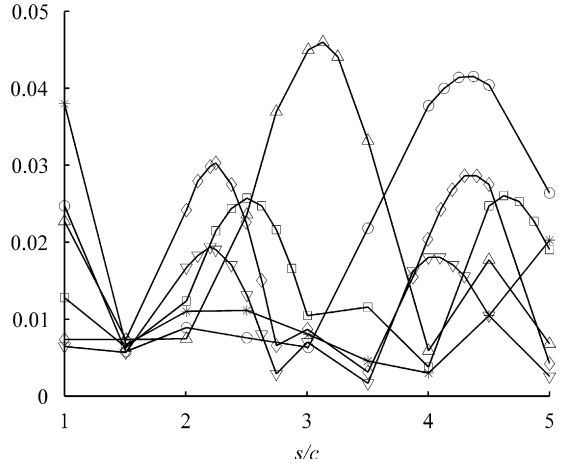

Fig. 2. Variations of root mean square lift with blade spacing for Cascade 1: (*) $c/d = 0.5$; (○) $c/d = 0.69$; (△) $c/d = 1$; (□) $c/d = 1.25$; (◇) $c/d = 1.4$; and (▽) $c/d = 1.43$.

reaches a minimum at $s/c = 4$ and rises again thereafter. The $(C_L)_{\text{rms}}$ variation is well within 0.04 and shows no significant peak. At $c/d = 0.69$, the aerodynamic resonant $(C_L)_{\text{rms}}$ peak occurs at $s/c = 4.25$, but a minimum response shows up at $s/c = 3$. As the frequency of the oncoming KVS excitation increases up to $c/d = 1$, the resonant peak appears to occur at a lower value of $s/c = 3.1$. This shows that a relatively compact cascade is more responsive to wake excitation generated from a rotor operating at high speed.

As c/d further increases to 1.25, the blade response shows two $(C_L)_{\text{rms}}$ peaks, one at $s/c = 2.5$ and another at 4.6. The two resonant peaks have comparable $(C_L)_{\text{rms}}$ amplitudes but their amplitudes are only 62% of that occurring at $c/d = 1$. Such change may imply a change of fluid–structure interaction mode of the cascade. The two peaks move to lower s/c values with an increase in c/d. A distribution of the aerodynamic resonance peaks of $(C_L)_{\text{rms}}$ with c/d at different values of s/c clearly indicates that the combined effects of upstream excitation frequency and the neighboring blades have a strong influence on the occurrence of aerodynamic resonance of the central blade in a rigid cascade. In general, the distribution of $(C_M)_{\text{rms}}$ of Cascade 1 shows similar trend to that of $(C_L)_{\text{rms}}$. Therefore, their plots are not shown in this paper; details are given in Lau [21].

In the isolated blade case [5], aerodynamic off-resonance phenomenon occurs at $c/d = 1$ and 2, while aerodynamic resonance phenomenon appears at $c/d = 0.5$, 1.5, 2.5, etc. For the cascade case, an obvious peak in the aerodynamic response is observed at $c/d = 1$. This indicates that, in the cascade case, even though the external wake disturbance includes an off-resonance excitation frequency, the coupling effect of the neighboring blade contributes to the strong fluid–structure interaction observed. This could increase the fluctuation level of the aerodynamic loads acting on the blade in a cascade. Looking at the $c/d = 0.5$ case, although this frequency leads to aerodynamic resonance in the isolated blade case, the cascade result shows that the variation of s/c could give rise to a significant reduction on the level of the fluctuation amplitude of the aerodynamic response. In other words, with an optimal choice of s/c in a cascade, the coupling effect of s/c and c/d could dampen the inherent rapid unsteady aerodynamic blade loading induced by the vortical excitation with an aerodynamic resonance frequency.

4.2. Fluid–structure interaction effect in Cascades 2 and 3

In Cascade 2, flow-induced vibration is present because the central blade is elastic and its neighboring four blades are rigid. Therefore, both aerodynamic and structural dynamic response of the central blade is present. However, the influence of vibrating neighboring blades on the central blade cannot be examined. The effect of vibrating neighboring blades is investigated using Cascade 3 where the three central blades are elastic.

The elastic central blade in Cascade 2 responds to the action of aerodynamic forces induced by the KVS vortices. Due to the coupled motion, the aerodynamic and structural response is largely dependent on c/d, and

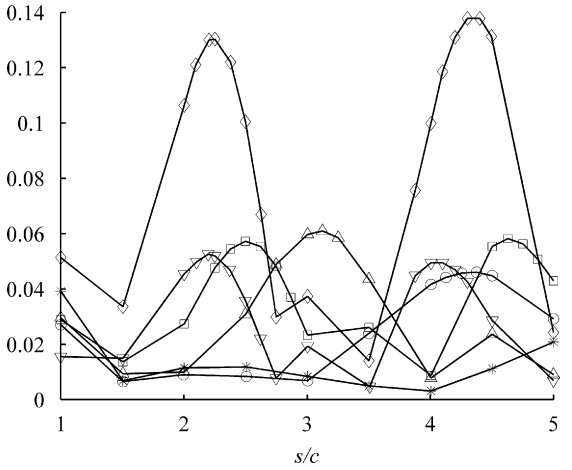

Fig. 3. Variations of root mean square lift with blade spacing for Cascade 2: (*) $c/d = 0.5$; (○) $c/d = 0.69$; (△) $c/d = 1$; (□) $c/d = 1.25$; (◇) $c/d = 1.4$; and (▽) $c/d = 1.43$.

the spacing of the neighboring blades, which impose a different boundary constraint on the elastic blade. As a result, the distributions of $(C_L)_{\mathrm{rms}}$ of Cascade 2 are different from those of Cascade 1 (Fig. 2).

Comparing Fig. 2 with Fig. 3, it can be seen that the difference in stiffness of the central blade does not significantly alter the overall behavior of the $(C_L)_{\mathrm{rms}}$ distribution. Maximum $(C_L)_{\mathrm{rms}}$ of Cascade 2 occurs at the same values of s/c as that of Cascade 1. The similarity of the $(C_L)_{\mathrm{rms}}$ distribution of Cascades 1 and 2 indicates that a major effect of fluid–blade interaction is to influence the aerodynamic response and the critical parameters for aerodynamic resonance to occur. However, the variation of the amplitude of $(C_L)_{\mathrm{rms}}$ of Cascade 2 differs greatly from Cascade 1. It can be seen from these two figures that the amplitude of $(C_L)_{\mathrm{rms}}$ for Cascade 2 is in general higher than that shown for Cascade 1 for all c/d values studied. This can be attributed to the effect of flow-induced vibration on the central blade of Cascade 2. Furthermore, the peak $(C_L)_{\mathrm{rms}}$ values of Cascade 2 now occurs at a higher KVS frequency ($c/d = 1.4$), with an amplitude approximately 2.7 times stronger than that at $c/d = 1$ of Cascade 1. This phenomenon is similar to the structural resonance reported in the studies of So et al. [5] and Leung and So [17] who showed that, as a result of coupled fluid–blade interaction, peak aerodynamic and structural response of an isolated elastic blade under KVS excitation occurs at $c/d = 1.4$, a value very close to the normalized structural natural frequency *in vacuo* of 1.666. Similar observation can also be made from the moment coefficient distribution which is not shown.

The rigid neighboring blades do not seem to have a significant effect on the structural resonance of the central blade. Consequently, structural resonance occurs at the same c/d as in the case of an isolated blade; i.e. the blade attains its highest amplitude of plunging and pitching at $c/d = 1.4$ during structural resonance. Since the distributions of $(h)_{\mathrm{rms}}$ and $(\theta)_{\mathrm{rms}}$ of the central blade with s/c and c/d parameters in Cascade 2 are very similar to those of Cascade 3, their details are not reported here.

For Cascade 3, the central three blades are all elastic while the outer two blades are rigid. That way, the effect of neighboring blade vibration on the aerodynamic and structural dynamic response of the central blade can be examined. The $(C_L)_{\mathrm{rms}}$, $(h)_{\mathrm{rms}}$ and $(\theta)_{\mathrm{rms}}$ distributions of the central blade of Cascade 3 are plotted in Fig. 4. It can be seen that the aerodynamic and structural dynamic response of the central blade for $s/c = 1.5$, 3.5 and 5 are relatively weak, and the amplitudes are approximately 10% of the peak values recorded at $s/c = 2.2$ and 4.4 for the $c/d = 1.4$ case. This finding indicates that, in a cascade, an optimal selection of s/c could diminish the influence arose from an external vortical excitation with a frequency inherently resonating with the blade structural dynamics. In addition, aerodynamic and structural resonance in Cascades 2 and 3 occurs at the same set of c/d and s/c parameters, with all peak values of $(C_L)_{\mathrm{rms}}$, $(h)_{\mathrm{rms}}$ and $(\theta)_{\mathrm{rms}}$ increased by different degrees. However, at each c/d case, the amplitude level difference of $(C_L)_{\mathrm{rms}}$, $(h)_{\mathrm{rms}}$ and $(\theta)_{\mathrm{rms}}$ between Cascades 2 and 3 is not significant, thus reflecting that the aerodynamic and structural dynamic response

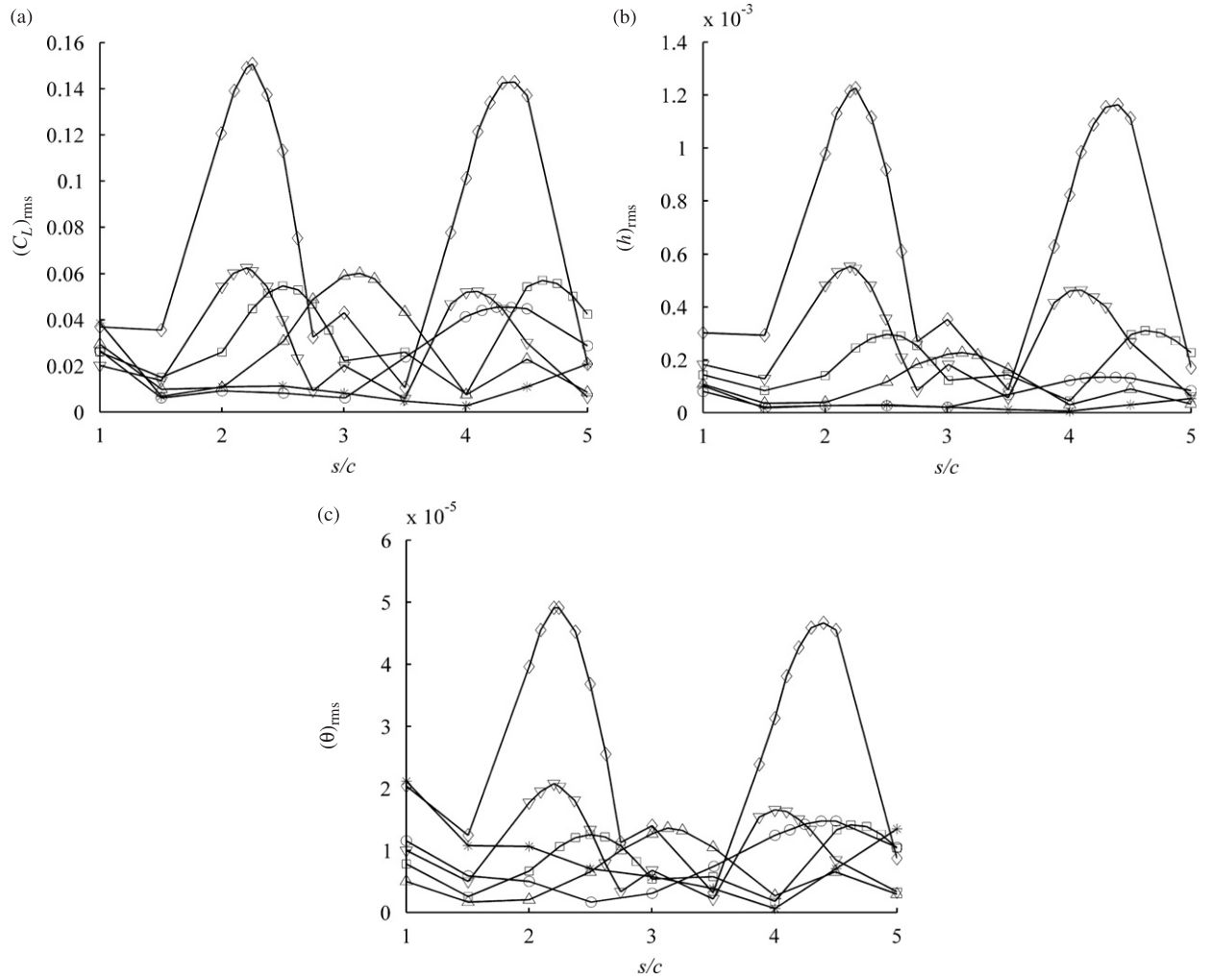

Fig. 4. Variations of root mean square (a) lift, (b) plunging displacement and (c) pitching displacement with blade spacing for Cascade 3: (*) $c/d = 0.5$; (○) $c/d = 0.69$; (△) $c/d = 1$; (□) $c/d = 1.25$; (◇) $c/d = 1.4$; and (▽) $c/d = 1.43$.

of the elastic central blade in a cascade are relatively insensitive to the vibrating motions of the neighboring blades.

4.3. Stable forced response of Cascades 2 and 3

Single and double peaks are observed in the variations of $(h)_{rms}$ and $(\theta)_{rms}$ with s/c for the cases of $c/d = 1$, 1.25 and 1.4 of Cascades 2 and 3 (Fig. 4). For each c/d case, the time-stationary variations of h and θ, their phase plane plots and spectra obtained from FFT analysis are shown in Figs. 5–9. Only the structural response of h and θ for the peak (or peaks) and minimum appeared in the curves of $(h)_{rms}$ and $(\theta)_{rms}$ versus s/c are illustrated in these figures. For the $c/d = 1$ case, only one peak is observed at $s/c = 3.1$ for both $(h)_{rms}$ and $(\theta)_{rms}$, while a minimum is found at $s/c = 4$. The h and θ time series, phase plane plots and spectrum of the peak and the minimum are shown in Figs. 5 and 6, respectively. For the $c/d = 1.25$ case, the behavior of $(h)_{rms}$ with s/c is similar to that of $(\theta)_{rms}$, with two peaks appearing at $s/c = 2.5$ and 4.6 and a minimum at $s/c = 4$. Similarly, for the $c/d = 1.4$ case, there are two peaks and one minimum in the $(h)_{rms}$ and $(\theta)_{rms}$ curves; the peaks occur at $s/c = 2.3$ and 4.4, and the minimum at $s/c = 3.5$. As the trends and variations of the time series, phase plane plots, and spectra of the two peaks and minimum, for $c/d = 1.25$ and 1.4 are similar, only the result of the $c/d = 1.4$ case is illustrated in Figs. 7–9.

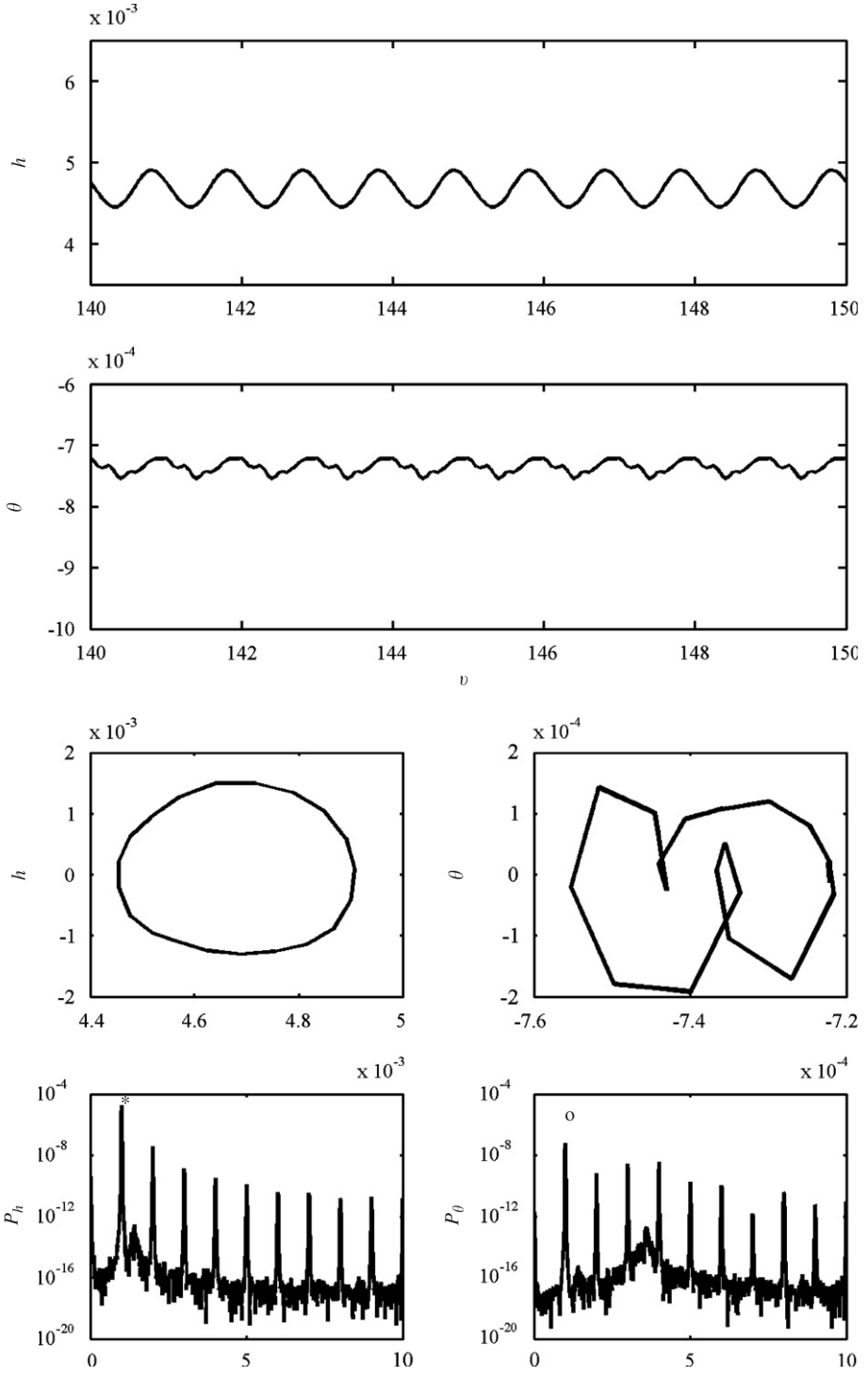

Fig. 5. Time series, phase plane plots and spectra of h and θ at peak response ($c/d = 1$, $s/c = 3.1$): (*) normalized first EIE mode plunging frequency = 1; and (○) normalized first EIE mode pitching frequency = 1.

The study of aerodynamic and structural resonance of an isolated blade subject to oncoming KVS excitation [5] reveals that the structural dynamic response of h and θ and their amplitudes are dependent on c/d. The maximum and minimum values of the fluctuating amplitude of the responses are bounded

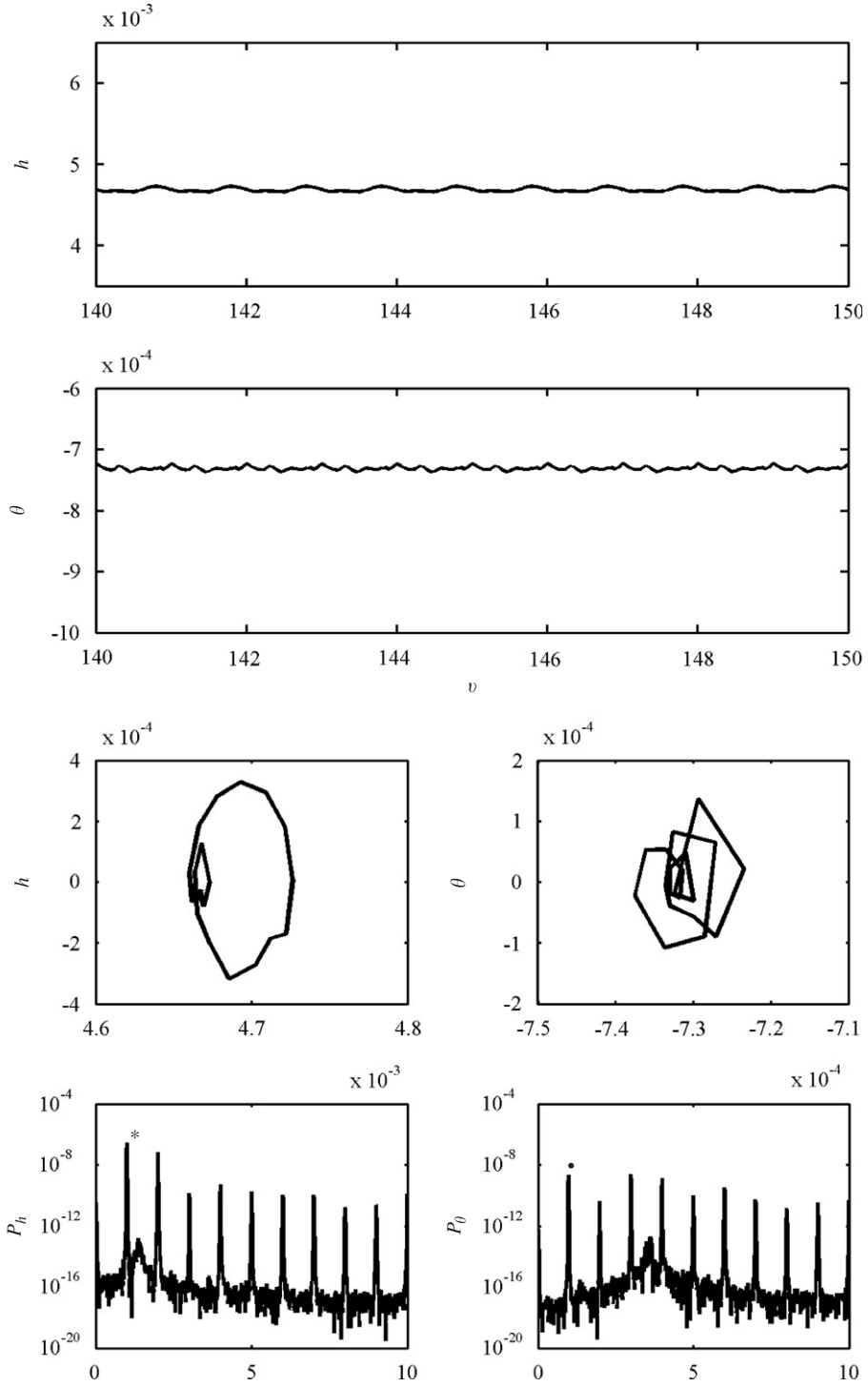

Fig. 6. Time series, phase plane plots and spectra of h and θ at minimum response ($c/d = 1$, $s/c = 4$): (*) normalized first EIE mode plunging frequency = 1; and (○) normalized first EIE mode pitching frequency = 1.

along the time axis. When neighboring blades are present, it can be seen from Figs. 5–9 that, in general, the structural dynamic response of h and θ of the central blade show stable flow-induced vibration behavior, the appearance of which could be attributed to the fact that although the blades in the

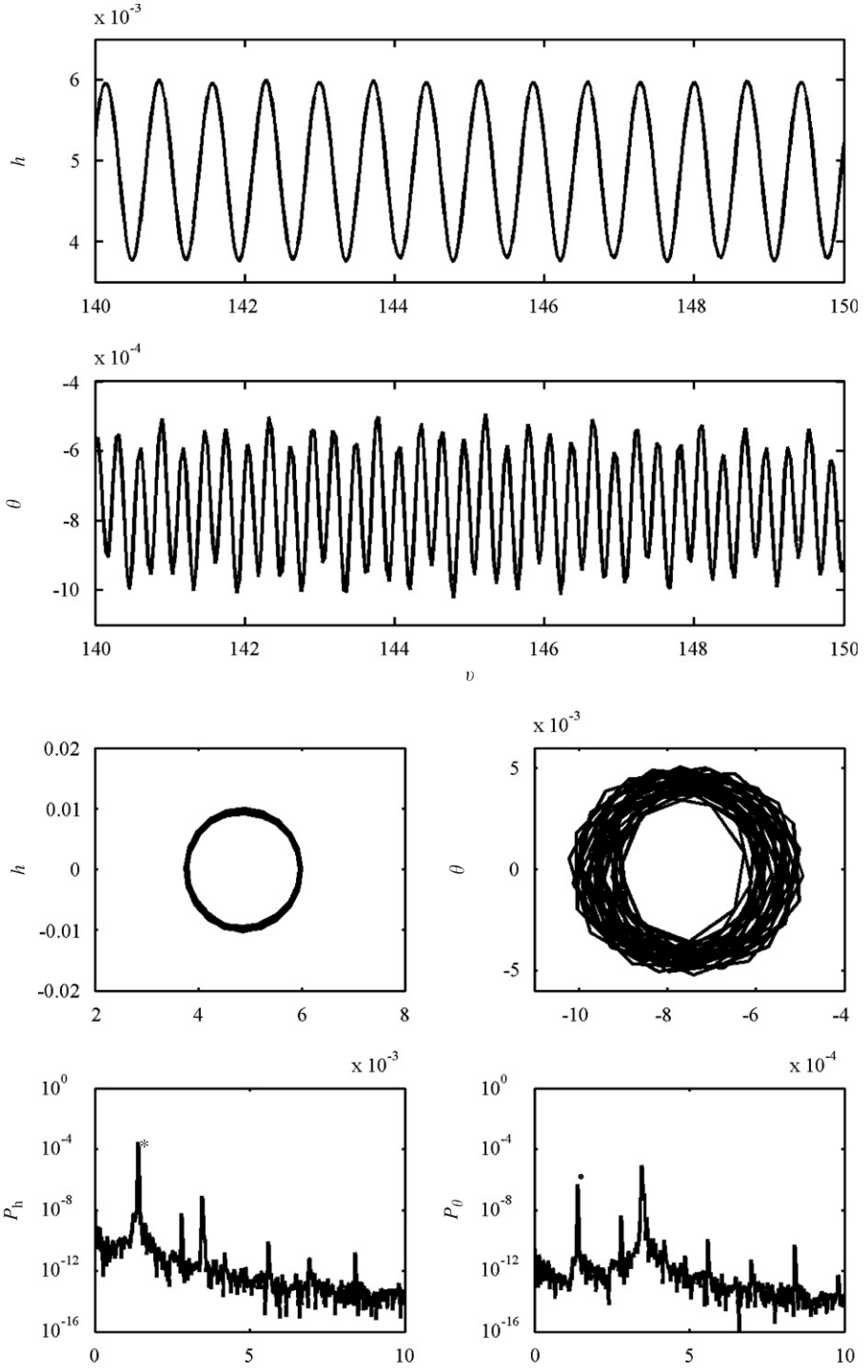

Fig. 7. Time series, phase plane plots and spectra of h and θ at first peak response ($c/d = 1.4$, $s/c = 2.3$): (*) normalized first EIE mode plunging frequency = 1.4; and (○) normalized first EIE mode pitching frequency = 1.4.

cascade are under continuous oncoming KVS excitation, the excitation is in fact limited by fluid damping that arises from fluid motion surrounding the blade and complicated fluid–cascade interaction. It is precisely this damping that limits the amplitude of oscillation of the central blade and consequently

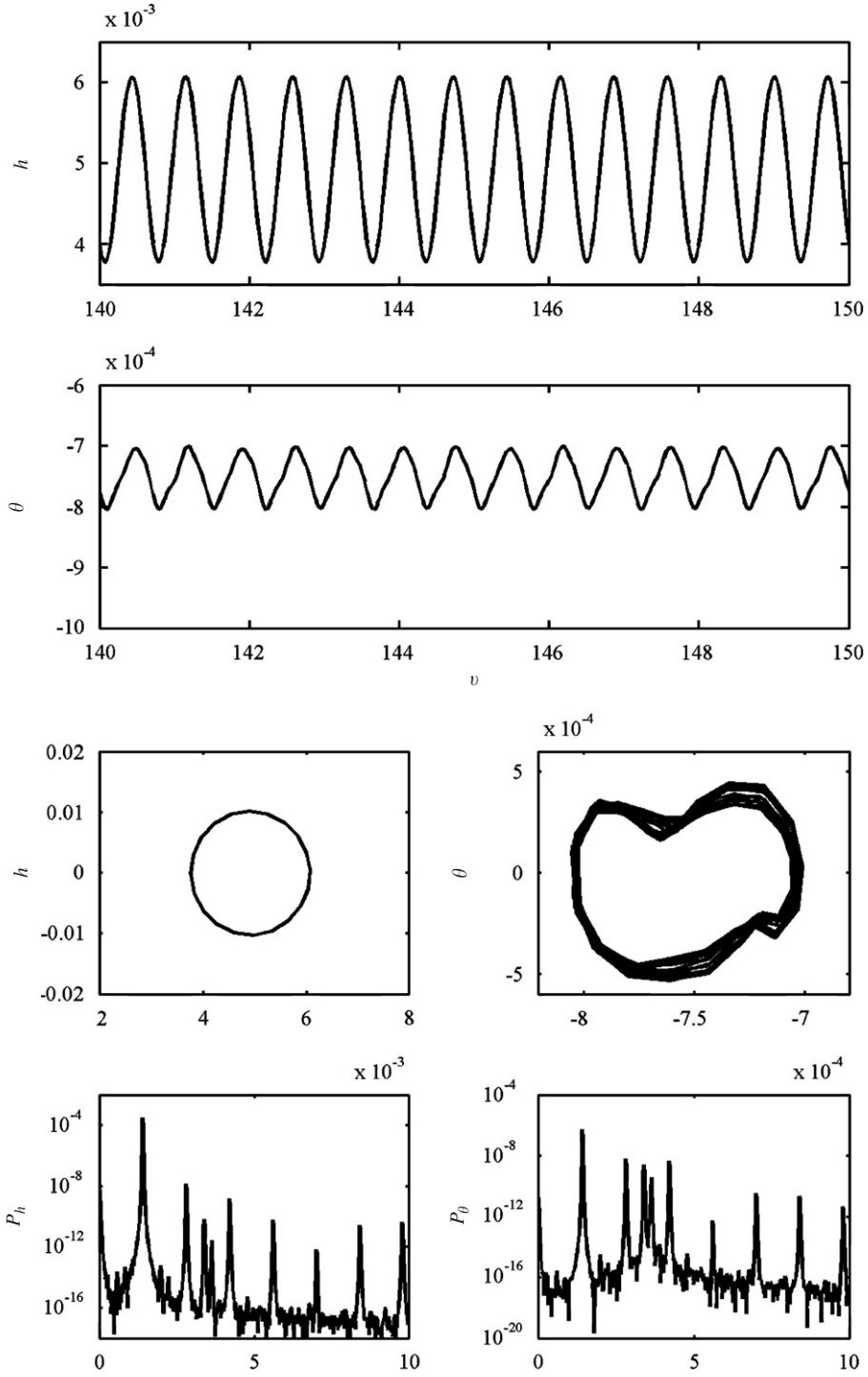

Fig. 8. Time series, phase plane plots and spectra of h and θ at second peak response ($c/d = 1.4$, $s/c = 4.4$): (*) normalized first EIE mode plunging frequency = 1.4; and (○) normalized first EIE mode pitching frequency = 1.4.

the occurrence of stable flow-induced vibration. The coupling effect of s/c and c/d does not appear to have much influence on the flow-induced vibration but does affect the amplitudes of the structural dynamic responses.

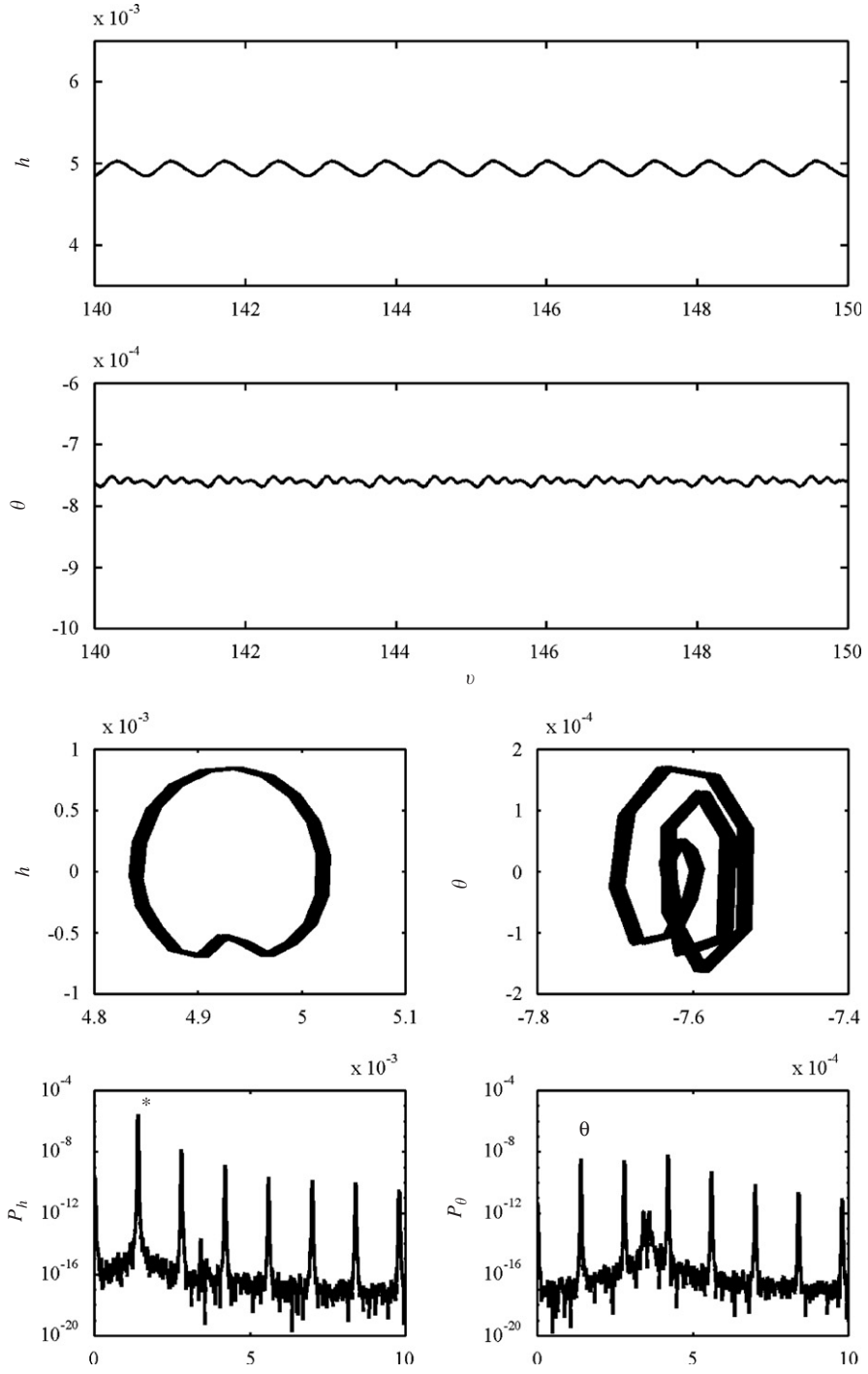

Fig. 9. Time series, phase plane plots and spectra of h and θ at minimum response ($c/d = 1.4$, $s/c = 3.5$): (*) normalized first EIE mode plunging frequency = 1.4; and (○) normalized first EIE mode pitching frequency = 1.4.

In the c/d cases examined, the phase plane plots of the plunging response (h versus $\dot{h}$) of the peak (or peaks) are essentially of circular shape with one or at most two loops, indicating the fundamental harmonic and the first mode of plunging (also see the corresponding spectrum) are the dominant frequencies (Figs. 5, 7 and 8). This shows that the fluid–structure system (at least the plunging response) is excited at resonance due to the

coupling effect of s/c and c/d. The phase plane plots of the pitching response (θ versus $\dot{\theta}$) show the superposition of several higher harmonics (Figs. 5, 7 and 8). The phase plane plots at the minimum shows that the stably forced plunging and pitching responses are composed of the fundamental and higher harmonics (Figs. 6 and 9). These results are useful in fatigue life analysis and the subsequent derivation of the design curves for axial flow turbomachines.

5. Vortex-induced vibration effect on HCF failure of turbine blade

The findings of the previous section show that if a stator is under the excitation induced by an oncoming rotor wake, the levels of the fluctuating aerodynamic and structural response of the stator blade depend critically on s/c and c/d. From Fig. 4, it can be seen that, in the cases of $c/d = 0.69$, 1, 1.25, 1.4 and 1.43, a single peak or multiple peaks are found in the variation of $(C_L)_{\text{rms}}$, $(C_M)_{\text{rms}}$, $(h)_{\text{rms}}$ and $(\theta)_{\text{rms}}$ with s/c. However, in each c/d case, the locations of the peak or peaks of $(C_L)_{\text{rms}}$, $(C_M)_{\text{rms}}$, $(h)_{\text{rms}}$ and $(\theta)_{\text{rms}}$ at the s/c axis are the same.

Figs. 10 and 11 show the contours of $(C_L)_{\text{rms}}$, $(h)_{\text{rms}}$, $(\theta)_{\text{rms}}$ and the respective estimated fatigue lives of the stator blade in a c/d versus s/c space. The two curves linked with asterisks show the loci of the peaks of

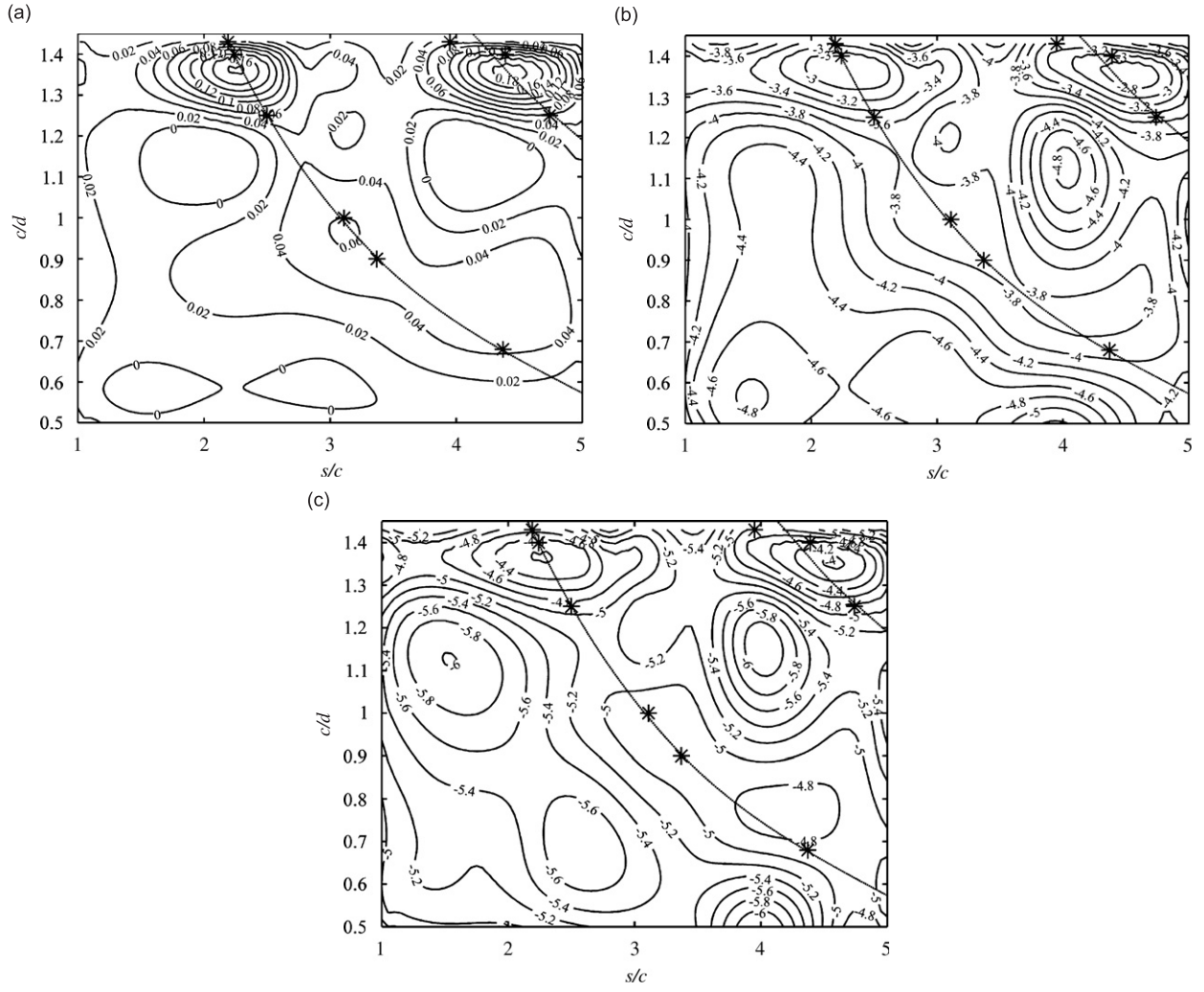

Fig. 10. Contours of aerodynamic and structural responses of the central blade in Cascade 3: (a) $(C_L)_{\text{rms}}$, (b) $(h)_{\text{rms}}$ in $\log_{10}$ scale, and (c) $(\theta)_{\text{rms}}$ in $\log_{10}$ scale. (....*....*....) Loci of peak responses.

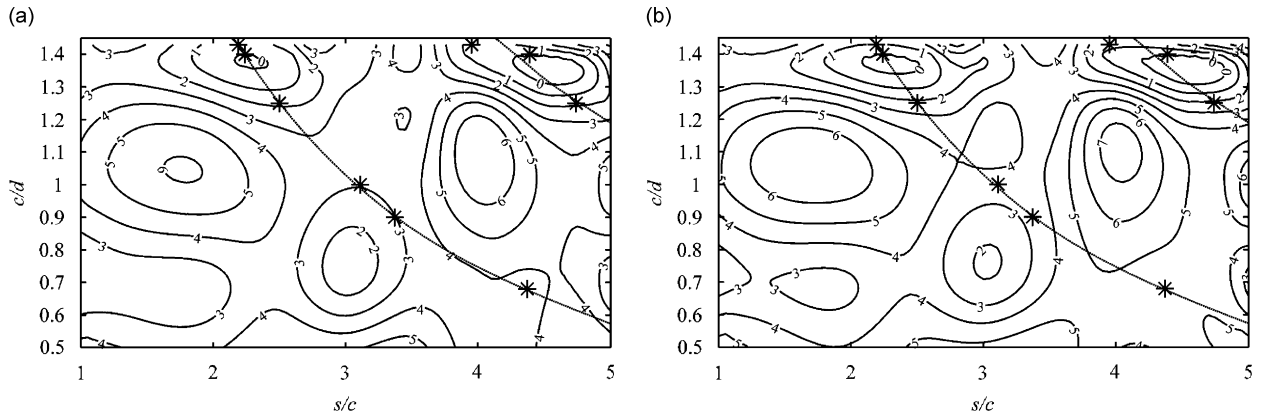

Fig. 11. Contours of relative fatigue life estimate, in $\log_{10}$ scale, of the central blade in Cascade 3: (a) by rainflow counting; and (b) by FFT-based spectral analysis. (....*....*....) Loci of relative minimum fatigue lives.

$(C_L)_{\text{rms}}$, $(C_M)_{\text{rms}}$, $(h)_{\text{rms}}$ and $(\theta)_{\text{rms}}$ and the minimum values of the estimated fatigue life of the blade. The case with $c/d = 1.4$ and $s/c = 2.25$ is chosen as the reference for the calculation of the relative fatigue lives of the central blade of Cascade 3 under different oncoming wake properties and stator row geometry for the formulation of the design curves. The calculated relative fatigue life based on the rainflow counting method and FFT analysis are compared in Fig. 11.

The figures indicate that, if a coupled rotor–stator pair is designed to operate with c/d and s/c values close to the loci of the peaks, the aeroelasticity of the stator blade becomes prominently unstable and the fatigue life of the stator blade is shorter. To improve the aeroelastic stability and fatigue life of the stator blade, the operational and geometric properties of a coupled rotor–stator pair should be properly designed so that the operating c/d and s/c values are far away from the loci of peaks. As an example, for a stator with $s/c = 4.5$ exposed to vortical disturbances propagated from the preceding rotor with $c/d = 1.4$ (this c/d value could lead to structural resonance), the corresponding fluctuating lift acting on the stator blade is approximately 0.07 (Fig. 10). The corresponding estimated relative fatigue life of the blade is about 1 cycle (it means that after the blade underwent one cycle of vibration, structural failure of the blade could occur), as shown in Fig. 11. However, if the frequency of the rotor is reduced by 57% and the corresponding c/d is reduced from 1.4 to 0.6, then the level of the fluctuating loads is reduced by 88%, while the fatigue life of the blade is extended by more than four orders of magnitude (Fig. 11a).

On the other hand, for a stator designed with a prescribed s/c, the design curves indicate that improper change of the rotor frequency could destabilize the aeroelastic stability as well as reduce the fatigue life of the stator blade. As an example, for a rotor–stator pair designed with $s/c = 2.5$ and $c/d = 1.15$, the corresponding fluctuating lift force acting on the stator blade is approximately 0.025 and the relative fatigue life of the blade is about $10^{3.3}$ cycles (from Figs. 10 and 11). However, if the rotor frequency is increased to $c/d = 1.25$, this leads to an increase of the vortical disturbance by about 9%. The design curves show that, such a slight increase in c/d double the level of the fluctuating lift force acting on the stator blade and a consequent reduction of the blade fatigue life by at least 1.6 orders of magnitude. Fig. 11 further shows that the levels and distributions of relative fatigue life computed from FFT analysis and rainflow counting are very similar. This suggests that, despite nonlinear fluid–structure interaction due to the oncoming wake, the dominant frequency plays a major role in determining the fatigue life of the vibrating stator blades, while the higher harmonics are much less significant.

The major difference between the properties of Cascades 1 and 3 is in the structural stiffness of the central blade; one with infinite stiffness (Cascade 1) and the other with finite stiffness (Cascade 3). The loci of the peaks of $(C_L)_{\text{rms}}$, $(C_M)_{\text{rms}}$, $(h)_{\text{rms}}$, $(\theta)_{\text{rms}}$ and the fatigue life of the central blade in Cascade 3, and those of $(C_L)_{\text{rms}}$ and $(C_M)_{\text{rms}}$ of the central blade in Cascade 1 are compared in the c/d–s/c space (Fig. 12). It can be observed that the loci for both Cascades 3 and 1 are coincident, indicating that the occurrence of peaks of the aerodynamic and structural dynamic response and the minima of the fatigue life of the stator blade is

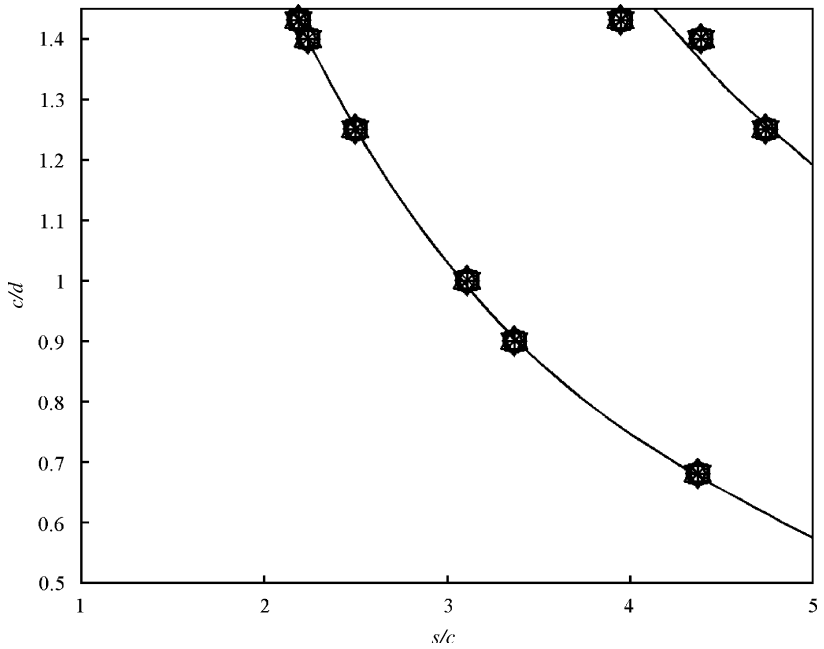

Fig. 12. Design curves for Cascade 3: (△) $(C_L)_{\mathrm{rms}}$ peaks; (▽) $(C_M)_{\mathrm{rms}}$ peaks; (○) $(h)_{\mathrm{rms}}$ peaks; (*) $(\theta)_{\mathrm{rms}}$ peaks; (+) minima of fatigue life; and for Cascade 1: (◇) $(C_L)_{\mathrm{rms}}$ peaks; (□) $(C_M)_{\mathrm{rms}}$ peaks.

insensitive to the structural stiffness of the stator blade. In addition, Fig. 12 outlines three distinct regions for the design of stator blades in a coupled rotor–stator pair with relatively more stable aeroelastic behavior and longer fatigue life span.

6. Use of present results with Campbell diagram

In engineering practice, the Campbell diagram is used to predict the operational conditions that could lead to resonant vibrations of the blade [2]. The methodology stems from the coincidence of the rotor-wake generated disturbances at WPF with any natural frequency of the stator blade. The prevention of resonant conditions is achieved by properly changing the rotational frequency of the rotor and its blade numbers to avoid any frequency coincidence. It should be noted that usually the natural frequencies of the stator blade are measured from an isolated blade *in vacuo*. However, in actual operation, a stator blade is in fact exposed to an entirely different environment due to the presence of neighboring blades and the complicated flows through the cascade. The design curves constructed in Fig. 12 raises some concerns on the use of the Campbell diagram for the prediction and prevention of blade structural resonance and HCF in rotor–stator interaction design.

In all cases studied, the stator blade in cascade displays structural resonance at a different frequency ($c/d = 1.4$) from the first mode *in vacuo* natural frequency ($c/d = 1.666$). This frequency shift is caused by fluid–structure interaction whose effect has been neglected in the construction of the Campbell diagram. Therefore, its use to design coupled rotor–stator vibration might not be appropriate. In addition, Figs. 3 and 4 indicate that even though the vertical disturbance carries a resonant frequency ($c/d = 1.4$) for the stator blade, optimal selection of blade spacing, $s/c = 3.5$ for example, can be made such that it could reduce the $(C_L)_{\mathrm{rms}}$ level of the stator blade by about 90% and its relative fatigue life cycle could be extended by up to 4.5 orders of magnitude. On the contrary, in case the vortical disturbance does not carry a resonant frequency, say $c/d = 1$, improper selection of blade spacing ($s/c = 3.1$) could lead to a level of $(C_L)_{\mathrm{rms}}$ that would excite the stator blade by a relative increase of five times and the fatigue life of the blade would reduce by three orders of magnitude.

The above observations indicate that the use of the Campbell diagram should be accompanied with information on the characteristics of aerodynamic/structural resonance as a result of the coupled

fluid–structure interaction. Therefore, Fig. 12 should be used in conjunction with the Campbell diagram if the effects of c/d and s/c were to be taken into account. It is in this sense that the Campbell diagram has been improved. Once fluid–structure interaction is taken into account in the design of stator blades, their resonant states and fatigue life due to HCF failure could be assessed more reliably.

7. Conclusions

Vortex-induced vibration of an elastic stator blade in a modeled rotor–stator pair has been numerically studied by examining the variations of blade response and resonance. A 2-D model of linear cascade, composed of five uniformly spaced high loading turbine blades, has been used and the focus is on the unsteady aerodynamic and structural response of the central blade. The oncoming rotor wake disturbance is simulated by six rows of alternating discrete KVS vortices superimposed on a uniform stream. The vortex spacing is selected to reflect the role of wake passing frequency (WPF). The unsteady flow field is assumed to be inviscid and incompressible, and a well-validated BEM code is employed to accurately resolve the coupled fluid–structure interaction of the cascade. Three different cascade configurations have been investigated: Cascade 1 has five rigid blades; Cascade 2 has one central elastic blade and four outer rigid blades; Cascade 3 has three central elastic blades and two outer rigid blades. The configurations are selected to allow the effects of fluid–structure interaction, vortex-induced vibration and the effects of vibrating neighboring blades to be examined systematically. This approach is not limited to the geometry of the high loading turbine blade considered. It is equally applicable to other blade geometries. Among the many parameters identified, two parameters, s/c and c/d, are found to be of importance in this fluid–structure interaction problem. The c/d parameter is chosen to represent the WPF characteristics found in a real rotor/stator situation, while s/c is related to the geometric design parameter of the stator.

From the results of Cascade 1 it can be deduced that, when a rigid cascade is excited by a c/d ratio that could give rise to aerodynamic resonance, changing s/c is able to reduce the level of the aerodynamic response effectively. Even though the rigid blades in the cascade are under a resonant external excitation, adjusting the blade spacing can affect the aerodynamic and structural dynamic response significantly. In turn, this leads to a reduction of the fluctuation amplitude. This behavior is independent of the stiffness of the neighboring blades. For Cascades 2 and 3, aerodynamic and structural dynamic responses of the central blade in the cascade are found to be a function of s/c and c/d; their relationships are nonlinear. As a result of the coupling effect of s/c and c/d, the vortex-induced excitation could drive the stator blade to a state of stable forced vibration. Its appearance is due to fluid damping which is derived mainly from fluid–structure interaction and is present even in an inviscid treatment of the problem. The coupling effect of s/c and c/d does not affect the LCO behavior but does affect the amplitude of the structural dynamic response. The behavior of the aerodynamic and structural dynamic response with various s/c is found to depend on c/d and the resulting fluid–structure interaction is rather insensitive to the effect of vibrating neighboring blades. However, the response due to aerodynamic and structural resonance is affected by c/d for a fixed blade spacing.

Since c/d and s/c are related to the operational conditions and geometry of the rotor–stator pair, design curves related to vortex-induced vibration and the corresponding relative HCF life estimate calculated from Miner's rule can be constructed using the aerodynamic and structural response data deduced from the cascade analysis. The design curves yield information that helps the selection of appropriate c/d and s/c values for a rotor–stator pair to minimize wake-induced vibration and maximize the fatigue life of the stator blade. In addition, the design curves constructed in the c/d–s/c space indicate that if the oncoming rotor wake carrying an excitation frequency that could resonate with the stator blade structure, varying s/c could alter the inherent resonance behavior of the stator blade. The vibration of the stator blade could be reduced significantly by a proper choice of s/c, even though the stator blade is under a resonant flow excitation. The design curves also shows that improper selection of s/c for a stator could increase the wake-induced vibration and reduce the fatigue life of the stator blade, even though the excitation frequencies of the oncoming rotor wake do not resonate with the natural frequencies of the stator blade.

Acknowledgement

The authors acknowledge funding support given by the Research Grants Council of the HKSAR under Grant nos. PolyU 5128/98E, PolyU 5161/00E and PolyU5272/04E.

References

[1] P.G. Hill, C.R. Peterson, *Mechanics and Thermodynamics of Propulsion*, second ed, Addison-Wesley Publishing Company, Inc., 1992, pp. 179–183, 311.
[2] T.S. Rao, *Turbomachine Blade Vibration*, Wiley, New York, 1991, p. 3, 292.
[3] K. Funazaki, T., Nishiyama, Measurements of simulated wake/rotor interaction phenomena in turbomachinery, *Unsteady Aerodynamic and Aeroelasticity of Turbomachines and Propellers*, *Proceedings of the Fifth International Symposium*, 1989, pp. 287–300.
[4] D.A. Topol, Rotor wake/stator interaction noise-predictions versus data, *Journal of Aircraft* 30 (1993) 728–735.
[5] R.M.C. So, I. Jadic, M.P. Mignolet, Fluid–structure resonance produced by oncoming alternating vortices, *Journal of Fluids and Structures* 13 (1999) 519–548.
[6] A.J. Sanders, S. Fleeter, Vane row indexing for passive vibration control of axial-flow turbomachine rotors, *Journal of Propulsion and Power* 15 (1999) 650–657.
[7] A.J. Sanders, S. Fleeter, Experimental investigation of rotor–inlet guide vane interactions in transonic axial-flow compressor, *Journal of Propulsion and Power* 16 (2000) 421–430.
[8] D.P. Probasco, J. Mitch Wolff, Axial spacing effects in a transonic compressor on the upstream vane loading, *International Journal of Turbo Jet Engines* 17 (2000) 197–206.
[9] P.J. Koch, D.P. Probasco, J. Mitch Wolff, W.W. Copenhaver, R.M. Chriss, Transonic compressor influences on upstream surface pressures with axial spacing, *Journal of Propulsion and Power* 17 (2001) 474–476.
[10] W.S. Yu, B. Lakshminarayana, Numerical simulation of the effects of rotor–stator spacing and wake/blade count ratio on turbomachinery unsteady flows, *Journal of Fluids Engineering* 117 (1995) 639–646.
[11] S. Fleeter, R.L. Jay, W.A. Bennett, Wake induced time-variant aerodynamics including rotor–stator axial spacing effects, *Journal of Fluids Engineering* 103 (1981) 59–66.
[12] G.L. Mellor, The aerodynamic performance of axial compressor cascade with application to machine design, Gas Turbine Laboratory Report No. 38, Massachusetts Institute of Technology, 1957.
[13] G.L. Mellor, The 65 Series Cascade Data, Gas Turbine Laboratory Report, Massachusetts Institute of Technology, 1958.
[14] J.C. Emery, L.J. Herrig, J.R. Erwin, A.R. Felix, Systematic two-dimensional cascade tests of NACA 65 series compressor blades at low speeds, NACA Report 1368, 1958.
[15] B.S. Yilbas, M.O. Budair, M. Naweed Ahmed, Numerical simulation of the flow field around a cascade of NACA 0012 airfoils—effects of solidity and stagger, *Computer Methods in Applied Mechanics and Engineering* 158 (1998) 143–154.
[16] W. Dobrzynski, Propeller noise reduction by means of unsymmetrical blade-spacing, *Journal of Sound and Vibration* 163 (1993) 123–136.
[17] R.C.K. Leung, R.M.C. So, Noise generation of vortex–blade resonance, *Journal of Sound and Vibration* 245 (2001) 217–237.
[18] I.A. Johnsen, R.O. Bullock, Aerodynamic design of axial low compressors, NASA Report SP-36, Washington, DC, 1965.
[19] S.C. Kacker, U. Okapuu, A mean line prediction method for axial flow turbomachine efficiency, *Journal of Engineering for Power* 104 (1982) 111–119.
[20] L. Fottner, Review on turbomachinery blading design problems, in: *Blading Design for Axial Turbomachines*, AGARD Lecture Series 167, 1989.
[21] Y.L. Lau, Experimental and Numerical Studies of Fluid–structure Interaction in Flow-Induced Vibration Problems, PhD Thesis, Department of Mechanical Engineering, The Hong Kong Polytechnic University, 2003.
[22] G.F. Wislicenus, *Fluid Mechanics of Turbomachinery, Vol. I*, McGraw-Hill, New York, 1965 237pp.
[23] C.G. Speziale, F. Sisto, S. Jonnavithulas, Vortex simulation of propagating stall in a linear cascade of airfoils, *Journal of Fluids Engineering* 108 (1986) 304–312.
[24] E. Naudascher, D. Rockwell, *Flow Induced Vibrations: An Engineering Guide*, A. A. Balkema, Rotterdam, 1994 3pp.
[25] H.P. Hodson, W.N. Dawes, On the interpretation of measured profile losses in unsteady wake–turbine blade interaction studies, *Journal of Turbomachinery* 120 (1996) 276–284.
[26] H.P. Hodson, R.J. Howell, Bladerow interactions, transition, and high-lift aerofoils in low-pressure turbines, *Annual Review of Fluid Mechanics* 37 (2005) 71–98.
[27] G. Cicatelli, C.H. Sieverding, The effect of vortex shedding on the unsteady pressure distribution around the trailing edge of a turbine blade, *Journal of Turbomachinery* 119 (1997) 810–819.
[28] C.H. Sieverding, H. Richard, J.M. Desse, Turbine blade trailing edge flow characteristics at high subsonic outlet Mach number, *Journal of Turbomachinery* 125 (2003) 298–309.
[29] C.H. Sieverding, H. Heinemann, The influence of boundary layer state on vortex shedding from flat plates and turbine cascades, *Journal of Turbomachinery* 112 (1990) 181–187.
[30] H.P. Hodson, An inviscid blade-to-blade prediction of a wake-generated unsteady flow, *Journal of Engineering for Gas Turbines and Power* 107 (1985) 337–344.

[31] T. Korakianitis, On the prediction of unsteady forces on gas turbine blades: part 1—description of the approach, *Journal of Turbomachinery* 114 (1992) 114–122.
[32] I. Jadic, R.M.C. So, M.P. Mignolet, Analysis of fluid–structure interactions using a time marching technique, *Journal of Fluids and Structures* 12 (1998) 631–654.
[33] M.A. Miner, Cumulative damage in fatigue, *Journal of Applied Mechanics* 102 (1945) A159–A164.
[34] W.J. Harris, *Designing Against Fatigue*, Chapman & Hall, New York, 1962 13pp.
[35] N.E. Dowling, Fatigue life prediction for complex load versus time histories, *Journal of Engineering Materials and Technology* 105 (1983) 206–214.
[36] American Society of Testing Materials ASTM E-1049, Standard practices for cycle counting in fatigue analysis, 1985 (Re-approved 1997).
[37] S.D. Downing, D.F. Socie, Simple rainflow counting algorithms, *International Journal of Fatigue* 4 (1982) 31–40.
[38] I.E. Treager, *Aircraft Gas Turbine Engine Technology*, second ed, McGraw-Hill, Inc., 1979, pp. 12, 15, 34, 41–42, 67–70, 184.
[39] Rolls-Royce plc., *The Jet Engine*, forth ed, The Technical Publications Department, Rolls-Royce plc., Derby, England, 1986, pp. 23, 58–59, 120–121.
[40] D.G. Wilson, T. Korakianitis, *The Design of High-Efficiency Turbomachinery and Gas Turbines*, second ed, Prentice-Hall, Inc., USA, 1998 288pp.
[41] C.E. Otis, P.A. Vosbury, *Aircraft Gas Turbine Powerplants*, Jeppesen, 2001 (Chapter 4).
[42] Y.L. Lau, R.M.C. So, R.C.K. Leung, Flow-induced vibration of elastic slender structures in a cylinder wake, *Journal of Fluids and Structures* 19 (2004) 1061–1083.
[43] K.F. Luk, R.M.C. So, R.C.K. Leung, Y.L. Lau, S.C. Kot, Aerodynamic and structural resonance of an elastic airfoil due to oncoming vortices, *AIAA Journal* 42 (2004) 899–907.